Ornithine Decarboxylase Promotes Catalysis by Binding the Carboxylate in a Buried Pocket Containing Phenylalanine 397†

Laurie K. Jackson,‡ Harold B. Brooks,§ David P. Myers,‡ and Margaret A. Phillips*,‡

Department of Pharmacology, The University of Texas Southwestern Medical Center at Dallas, 5323 Harry Hines Boulevard, Dallas, Texas 75390-9041, and Eli Lilly and Company, Lilly Corporate Center, Indianapolis, Indiana 46285

Received September 4, 2002; Revised Manuscript Received December 10, 2002

ABSTRACT: Ornithine decarboxylase (ODC) is a pyridoxal 5′-phosphate (PLP) dependent enzyme that catalyzes the decarboxylation of L-Orn to putrescine, a rate-limiting step in the formation of polyamines. The X-ray crystal structures of ODC, complexed to several ligands, support a model where the substrate is oriented with the carboxyl-leaving group buried on the *re* face of the PLP cofactor. This binding site is composed of hydrophobic and electron-rich residues, in which Phe-397 is predicted to form a close contact. Mutation of Phe-397 to Ala reduces the steady-state rate of product formation by 150-fold. Moreover, single turnover analysis demonstrates that the rate of the decarboxylation step is decreased by 2100-fold, causing this step to replace product release as the rate-limiting step in the mutant enzyme. These data support the structural prediction that the carboxyl-leaving group is positioned to interact with Phe-397. Multiwavelength stopped-flow analysis of reaction intermediates suggests that a major product of the reaction with the mutant enzyme is pyridoximine 5′-phosphate (PMP), resulting from incorrect protonation of the decarboxylated intermediate at the C4′ position. This finding was confirmed by HPLC analysis of the reaction products, demonstrating that Phe-397 also plays a role in maintaining the integrity of the reaction chemistry. The finding that the carboxylate-leaving group is oriented on the buried side of the PLP cofactor suggests that ODC facilitates decarboxylation by destabilizing the charged substrate carboxyl group in favor of an electrostatically more neutral transition state.

Ornithine decarboxylase (ODC)[1] is a pyridoxal 5′-phosphate (PLP) dependent enzyme that catalyzes the formation of the diamine, putrescine. This reaction is a rate-limiting step in the biosynthesis of polyamines, which are required for cell proliferation. ODC is the target of α-difluoromethylornithine (DFMO), a suicide inhibitor used to treat African sleeping sickness (*1*−*3*), which is a fatal tropical disease caused by infection with the parasitic protozoa *Trypanosoma brucei*.

PLP-dependent enzymes catalyze a variety of chemical reactions involving amino acids, including decarboxylation, transamination, racemization, and β- or γ-elimination (*4*). The PLP cofactor promotes catalysis by stabilizing carbanionic reaction intermediates and plays a large role in the rate acceleration achieved by these enzymes. Dunathan proposed that the specificity of the bond cleavage step for PLP-dependent enzymes is controlled by orientation of the scissile bond such that it is aligned with the π electrons of the imine double bond and oriented perpendicular to the PLP ring (*5*). This hypothesis has received support from both experimental (*6*−*9*) and computational studies (*10*). Interactions between the substrate and the apoenzyme are responsible for properly orienting the substrate to promote the physiological reaction chemistry. For the PLP-dependent decarboxylases it has been proposed that cleavage of the carboxylate leaving group would be promoted by binding to a nonpolar environment (*11*).

The proposed mechanism of decarboxylation catalyzed by ODC (Figure 1) is supported both by X-ray structural analysis (*12*−*15*) and by a number of mechanistic studies that have addressed the roles of active site residues (*13*, *16*−*19*). The PLP cofactor forms a covalent bond (internal aldimine) with the active site Lys-69 on native ODC. This bond is exchanged for an external aldimine with substrate by way of a *gem*-diamine intermediate in the first steps of the reaction. Electrons from the charged substrate carboxylate are delocalized into the PLP π system as decarboxylation occurs. These steps are followed by protonation at C_α, hydrolysis, and product release. In wild-type ODC the protonation step is tightly controlled, and off-pathway reactions caused by protonation at the C4′ position occur in only 0.01% of the turnovers (*13*).

Though a number of X-ray structures of mammalian (*14*, *15*) and *T. brucei* ODC [native, DFMO-inactivated, and complexed to putrescine (*12*, *13*)] have been solved, no structure directly demonstrates the position of the substrate

† This work was supported by grants (to M.A.P.) from the National Institutes of Health (R01 AI34432) and the Welch Foundation (I-1257) and by a predoctoral training grant (to L.K.J.) from the National Institutes of Health (T32 GM07062). M.A.P. is a recipient of a Burroughs Wellcome Fund Scholar Award in Molecular Parasitology.

* To whom correspondence should be addressed. Tel: (214) 648-3637. Fax: (214) 648-9961. E-mail: margaret.phillips@UTSouthwestern.edu.

‡ The University of Texas Southwestern Medical Center at Dallas.

§ Eli Lilly and Co.

[1] Abbreviations: ODC, *Trypanosoma brucei* ornithine decarboxylase; PLP, pyridoxal 5′-phosphate; PMP, pyridoxamine 5′-phosphate; DFMO, α-difluoromethylornithine; RT, retention time; λ_{ex} = excitation wavelength; λ_{em} = emission wavelength; γABA = γ-aminobutyraldehyde.

10.1021/bi026795z CCC: $25.00
Published on Web 02/14/2003

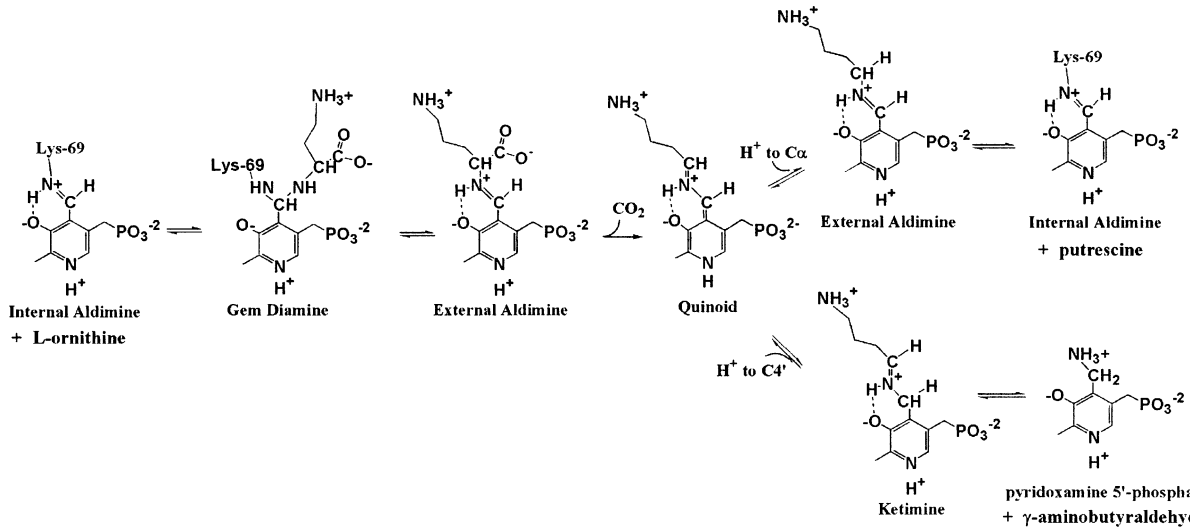

FIGURE 1: Reaction mechanism of ODC with L-Orn. Protonation at C_α produces the preferred product putrescine, while protonation at C4′ generates γABA and PMP in a off-pathway reaction.

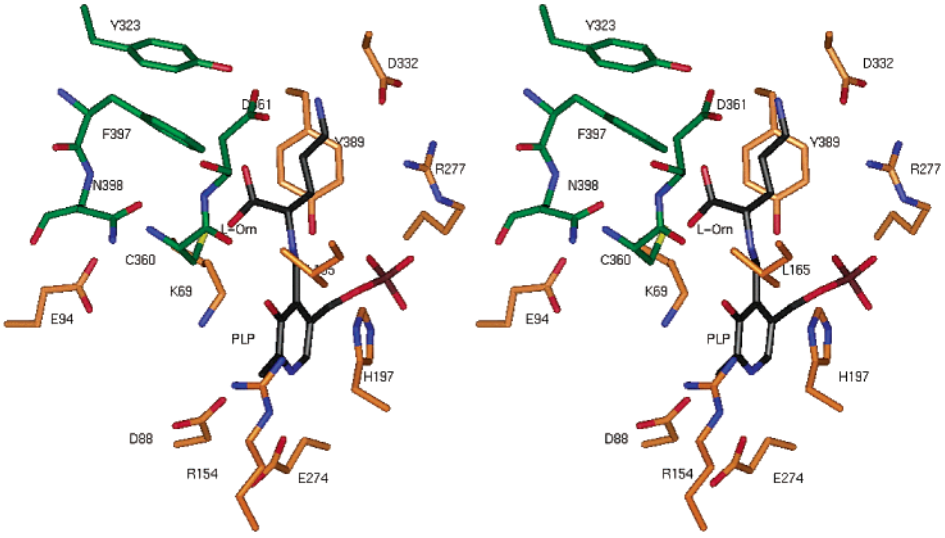

FIGURE 2: Model of the *T. brucei* ODC active site bound to L-Orn. The X-ray structure of *T. brucei* ODC complexed with putrescine (PDB ID code 1f3t) was used to model the position of the carboxyl group for L-Orn. The carboxylate was positioned onto the *re* face of the cofactor, perpendicular to the face of the ring. Residues predicted to be within 5 Å of the substrate carboxylate are displayed as a stereoview. For monomer A carbon atoms are in green, for monomer B carbon atoms are in orange, and the carbon atoms of PLP and L-Orn are colored black. Nitrogen atoms are in dark blue, oxygens are in red, sulfurs are in yellow, and phosphates are in brown. C360 and D361 are in the foreground relative to L-Orn. These models are displayed with InsightII, version 97.0 (Accelrys, San Diego, CA).

carboxylate in the L-isoform. Possible binding positions for the substrate carboxylate on ODC are limited by the necessity for the leaving group to be perpendicular to the PLP ring (*5*). The carboxylate of the substrate could potentially either be bound on the solvent-exposed *si* face of the cofactor or be buried in the active site pocket on the *re* face. The available structural evidence favors the *re* position for the substrate carboxylate. During inactivation of ODC by DFMO, decarboxylation with the loss of a fluoride anion generates a conjugated amine (*21*). Nucleophilic attack of this species by Cys-360 displaces the second fluoride and generates a covalent bond with the inhibitor and a prochiral C_α center. DFMO positioned with the carboxylate oriented on the *re* face would generate a conjugated amine in position for direct attack by Cys-360, while the opposite orientation would require significant rotation to be positioned for attack. Consistent with this analysis, a recently refined structure of *T. brucei* ODC bound to D-Orn demonstrates that for this isomer the carboxylate is oriented on the *si* face of PLP, thus suggesting that the L-isomer will bind on the opposite side of the cofactor (*20*).

On the basis of these structural observations L-Orn was modeled into the *T. brucei* ODC active site (Figure 2). The model predicts that the carboxylate binding site will include several hydrophobic residues (Phe-397, Tyr-389, and the hydrophobic side chain of Lys-69), as well as Asp-361. Neither the electrostatics nor the hydrophobic nature of these amino acids favors the binding of the negatively charged CO_2 group, suggesting that this pocket would facilitate decarboxylation by destabilizing the ground-state structure in favor of the more neutral transition state. To investigate the role of hydrophobic residues in promoting decarboxylation, the F397A mutant of *T. brucei* ODC was studied by steady-state and pre-steady-state kinetic methods. Single turnover analysis suggests that the mutation significantly lowers the rate of the decarboxylation step and that, unlike

for the wild-type enzyme, this step is now rate limiting. These data establish a role for Phe-397 in promoting the chemistry of the decarboxylation step, supporting the hypothesis that ODC binds the leaving group on the *re* face of the cofactor. In addition, the mutant enzyme is no longer capable of maintaining strict reaction specificity, and 34% of the decarboxylation events result in the formation of deaminated product. Phe-397 thus likely plays an additional role in promoting the proper reaction chemistry during the protonation step.

EXPERIMENTAL PROCEDURES

Materials

[1-$^{14}CO_2$]-L-Orn (56 mCi/mmol, 0.02 mM) was purchased from Amersham. HPLC-grade acetonitrile, triethylamine, buffers, PLP, and pyrrolidine were purchased from Sigma.

Methods

Modeling of L*-Orn into the ODC Active Site.* Molecular coordinates from the X-ray crystal structure of *T. brucei* ODC complexed with putrescine (PDB ID code 1f3t) were used to model the L-Orn carboxylate onto putrescine. The carboxyl group was oriented perpendicular to PLP on the *re* face. The structure was displayed in InsightII version 97.0 (Accelrys, San Diego, CA). Hydrogens were added to putrescine using the biopolymer module of InsightII, and the carboxylate was modeled using the position of the *re* face putrescine C_α hydrogen, again using the biopolymer to form the bond. The torsion angle around the $C_\alpha-CO_2$ bond of the modeled L-Orn was rotated manually in Insight II to minimize steric conflicts with active site residues.

Site-Directed Mutagenesis, F397A ODC Expression, and Purification. The creation of the F397A *T. brucei* ODC clone was previously described (*22*). The mutant protein was purified as described for wild type (*16*, *23*) in yields of more than 150 mg/L.

Steady-State Analysis of the Reaction of L*-Orn with F397A ODC by Determination of CO_2 Production.* The steady-state analysis of F397A ODC has been described previously (*22*). A spectrophotometric assay that couples CO_2 production to the oxidation of NADH was used to follow the steady-state decarboxylation reaction (*23*). The reaction of F397A ODC (3−12 μM) with L-Orn (0.1−8.0 mM) in the presence of excess (50 μM) PLP was monitored at 37 °C.

Single Turnover Kinetic Analysis of the Reaction of F397A ODC with L*-Orn.* [^{14}C]-L-Orn (3 μM) was incubated with a molar excess of F397A *T. brucei* ODC (12.5−800 μM) at 37 °C in 0.1 M Hepes, pH 7.5, for 0−5 min. The reactions were quenched with an equal volume of 2 M NaOH and 50 mM cold L-Orn. Reactions were acidified with an equal volume of concentrated HCl, and $^{14}CO_2$ was allowed to evolve at room temperature overnight before the radioactivity remaining in solution was quantified. The data were fitted to the equation describing a single exponential decay (eq 1, where $N = 1$) to obtain k_{obs} for each ODC concentration. The enzyme concentration dependence of k_{obs} was fitted to eq 2 to determine k_{decarb} and $K_{M,decarb}$.

$$y = b + \sum_{I=1}^{N} c_i e^{-k_i t} \quad (1)$$

$$k_{obs} = \frac{k_{decarb}[E]}{K_{M,decarb} + [E]} \quad (2)$$

Pre-Steady-State Kinetic Analysis by UV−Vis Stopped-Flow Spectroscopy. F397A ODC (40 μM final) was mixed with L-Orn (0.12−45 mM final) in 0.1 M Hepes, pH 7.5, and 2 mM glutathione. Reactions proceeded at 37 °C and were monitored using a Biologic SFM3 mixer with a TC-100 (1 cm path length) quartz cell coupled to a BioKine PMS-400. Data were collected at 420 nm from 3 ms to 20 s. A spectrum was collected every 0.2 ms for the first 15 ms, every 1 ms for the next 385 ms, and every 50 ms for the next 19600 ms. The dead time was 3 ms at a flow velocity of 12 mL/s. Single wavelength data were analyzed using Biokine 2.02 (Biologic, Claix, France) to determine the observed rate constants, k_{obs}, using eq 1.

For multiwavelength data collection the mixer was coupled to a J&M Tidas16 256 diode array (Molecular Kinetics, Pullman, WA) as described (*16*). Data were collected over 310−500 nm for 3−28950 ms. A spectrum was collected every 1 ms for the first 156 ms, every 7 ms for the next 861 ms, every 27 ms for the next 3942 ms, and every 124 ms for the next 23991 ms. The dead time was 3 ms at a flow velocity of 12 mL/s. Multiwavelength data were analyzed using Specfit 2.12 (Spectrum Software Associates, Chapel Hill, NC) to determine the observed rate constants, k_{obs}, as described (*13*).

Chromatographic Determination of the Steady-State Rate of Product Formation by F397A ODC. F397A *T. brucei* ODC (60 μM) was incubated at 37 °C with 3 mM L-Orn (pH 7.5) in 15 mM potassium phosphate (pH 7.4), 3 mM PLP, and 1 mM DTT for a range of times ($t = 0$ to $t = 4$ min), and the reaction was quenched with 6.7% TCA. Samples were reduced with 10 mg/mL $NaBH_4$ and derivatized with an Acc Q-Fluor reagent kit (Waters, Milford, MA) as described (*13*). Derivatized ligand was separated by HPLC using an AccQ·TAG column (Waters, Milford, MA). The column was preequilibrated with 80% eluent A (17 mM triethylamine, 140 mM sodium acetate, pH 5.04) and 20% eluent B (100% acetonitrile), and the derivatized product was eluted under the same conditions. The column was calibrated using the retention times of the following reduced and derivatized standards (12−60 pmol): pyrrolidine (RT = 7.5 min) and putrescine (RT = 11.15 min). The concentrations of products were determined by intergrating the area under the curve for each peak and comparing these values to a standard curve generated from known concentrations of products. Peaks were monitored with a Rainin Dynamax fluorescence detector, Model FL-1 (λ_{ex} = 250 nm, λ_{em} = 395 nm). Reactions with at least three turnovers but less than 20% L-Orn depletion were analyzed to obtain rates.

RESULTS

Modeling of L*-Orn into the ODC Active Site.* The L-Orn carboxylate was modeled into the active site of *T. brucei* ODC using the structure of the enzyme bound to the product putrescine (Experimental Procedures). The CO_2 group was inserted onto the C_α of putrescine on the *re* face of the PLP cofactor, oriented perpendicular to the plane of the ring, to create L-Orn in the active site (Figure 2). This model places the carboxylate in a buried site with several hydrophobic

Table 1: Results from Steady-State and Pre-Steady-State Kinetic Analysis of the ODC Reaction with L-Orn[a]

enzyme	F397A ODC	wild-type ODC
(A) Steady-State Decarboxylation Rates		
k_{cat} (s^{-1})	0.059 ± 0.001	9.4[b]
K_M (mM)	0.37 ± 0.20	0.5[b]
(B) Steady-State Product Formation Measured by HPLC		
$v_{total\ product\ formed}$ (s^{-1})	0.044 (100%)	
$v_{putrescine}$ (s^{-1})	0.029 (66%)	11[c] (100%)
$v_{\gamma ABA}$ (s^{-1})	0.015 (34%)	
(C) Single Turnover Analysis		
k_{decarb} (s^{-1})	0.066 ± 0.003	150[c]
$K_{M,decarb}$ (mM)	0.050 ± 0.07	0.57[c]
(D) Pre-Steady-State Single Wavelength Analysis of the Reaction of L-Orn (22.5 mM) with F397A ODC		
k_{obs1} (s^{-1})	23 ± 1	
k_{obs2} (s^{-1})	0.079 ± 0.003	

[a] All data were collected at 37 °C. Reported errors for (A)−(C) are the standard errors of the fit; for (D) errors are the standard deviation of the mean ($n = 3$). [b] Data were taken from ref *14*. [c] Data were taken from ref *9*.

groups (Phe-397, Tyr-389, Tyr-323, and the methylene carbons of Lys-69) and with Asp-361 (Figure 2). The closest predicted contacts are to Phe-397, to the methylene carbons of Lys-69, and to Asp-361. Cys-360 also forms close contacts to the modeled carboxylate; however, this residue has been observed in multiple conformations in the structures of native ODC versus the structures liganded with DFMO or putrescine (*12*, *13*). These data suggest that rotation around the C_β atom of Cys-360 could readily occur to accommodate the carboxylate moiety. Lys-69 forms interactions with the substrate carboxylate through the methylene groups of its side chain; the Lys-69 N_ϵ-amino group in the liganded structure is turned out of the pocket to interact with Asp-88 and Glu-94 and does not appear in position to form H-bonding interactions with the substrate carboxylate. Asp-361, while close to the predicted CO_2 binding site, also forms a through-water interaction with the δ-amino group of substrate and has been demonstrated to be essential for substrate binding (*12*, *17*).

Overall, the predicted substrate carboxylate binding site is composed of hydrophobic and electron-rich residues that would provide unfavorable interactions with the charged substrate carboxylate. Lys-69 has already been demonstrated to have an essential role both in Schiff base formation and in the decarboxylation step (*19*). The prediction that Phe-397 forms a major component of the carboxylate binding site suggests that this residue will also play an important role in promoting decarboxylation. To provide additional evidence for the predicted carboxylate binding site and to investigate the role of Phe-397 in the chemistry of the ODC reaction, the Ala mutant of Phe-397 (F397A ODC) was characterized by pre-steady-state and single turnover kinetic analysis.

Steady-State Rate of the Reaction of L*-Orn with F397A ODC.* Steady-state analysis of F397A ODC was previously reported by our laboratory (*22*). The steady-state rate of the decarboxylation of L-Orn by F397A ODC ($k_{cat} = 0.06\ s^{-1}$) is reduced by 150-fold compared to the wild-type enzyme, while the K_M for the reaction was not affected (Table 1).

*Single Turnover Kinetic Analysis of F397A ODC with [1-$^{14}CO_2$]-*L*-Orn.* Single turnover kinetics provides information on the reaction steps up to and including the first irreversible step. These steps in the ODC reaction mechanism potentially include Schiff base formation and decarboxylation (Figure 1). Kinetic steps following decarboxylation (e.g., protonation and product release) do not contribute to the single turnover kinetics. For wild-type ODC, the data suggest that the single turnover rate reflects the decarboxylation step (*13*, *16*).

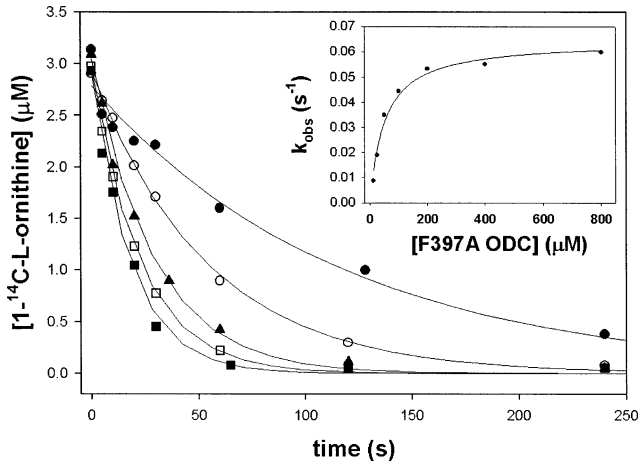

FIGURE 3: Single turnover data for the reaction of F397A ODC with L-Orn. [1-^{14}C]-L-Orn (3 μM) was reacted at 37 °C with ODC at multiple enzyme concentrations: (●) 12.5 μM, (○) 25 μM, (▲) 50 μM, (□) 100 μM, and (■) 400 μM. The decrease in radioactivity resulting from the loss of $^{14}CO_2$ from solution was followed over time. The data were fitted to eq 1 ($N = 1$) to determine the observed rate constant (k_{obs}). k_{obs} obtained from each concentration of ODC were fitted to eq 2 (inset) to obtain k_{decarb} and $K_{M,decarb}$ (Table 1). Data points are shown as filled circles, and fits to the data are displayed as lines.

The reaction of F397A *T. brucei* ODC (12.5−800 μM) with [1-$^{14}CO_2$]-L-Orn (3 μM) was followed under single turnover conditions at 37 °C. The $^{14}CO_2$ formed during the reaction was evolved from solution under acidic conditions, allowing the progress of the reaction to be followed by monitoring the loss of radioactivity in solution (Figure 3). The data obtained demonstrated first-order kinetics and were fitted to eq 1 ($N = 1$) to obtain the observed rate constant (k_{obs}). This reaction was followed at multiple enzyme concentrations, and the data were fitted to eq 2 to obtain k_{decarb} and $K_{M,decarb}$ (Table 1). Compared with the wild-type enzyme, k_{decarb} for F397A ODC (0.07 s^{-1}) is reduced by 2100-fold. The rate constant k_{decarb} represents the overall catalytic rate of the reaction through the decarboxylation step. The decarboxylation rate obtained from this single turnover analysis is similar to the overall steady-state rate of 0.06 s^{-1}, thus demonstrating that this step has become rate limiting in the mutant enzyme. This result is in contrast to the wild-type enzyme where product release is the rate-limiting step of the steady-state reaction (*13*, *16*).

Pre-Steady-State Kinetic Analysis by Multiwavelength and Single Wavelength Stopped-Flow Spectroscopy of the Reaction of F397A ODC with L*-Orn.* The absorbance spectrum of PLP is sensitive to the electronic and tautomeric state of the cofactor, and the formation and decay of reaction intermediates can be monitored spectrally by stopped-flow methods (*13*, *16*). The reaction of F397A ODC (40 μM) with L-Orn (22.5 mM) was followed by multiwavelength (310−500 nm) stopped-flow spectroscopy under pre-steady-state conditions (Figure 4). The first observed phase is character-

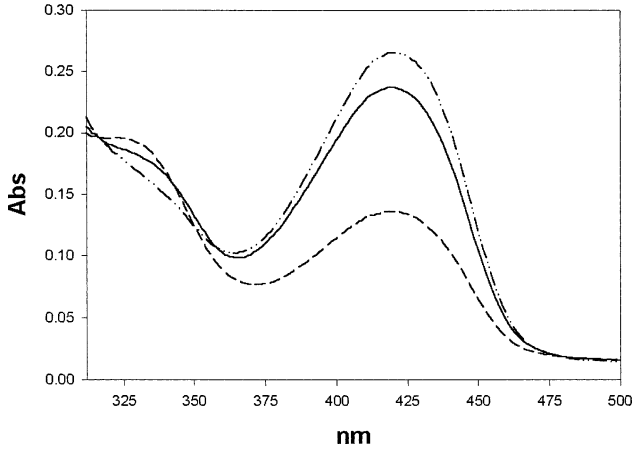

FIGURE 4: Multiwavelength kinetic analysis of the reaction of F397A ODC with L-Orn. Representative spectra (310−500 nm) at selected time points are displayed at 3 ms (solid line), 252 ms (dashed and dotted line), and 28 s (dashed line) after rapid mixing of enzyme (40 μM) and substrate (22.5 mM L-Orn) at 37 °C.

ized by an increase at 420 nm and a decrease at 330 nm and the second by a decrease in the 420 nm signal and an increase at 330 nm. The spectral properties of the initial species are characteristic of a Schiff base as previously reported for the wild-type enzyme (*16*). The spectral characteristics of the cofactor observed at the end of the reaction suggest that a ketimine intermediate has formed similar to what was observed for the C360A and C360S mutant ODCs (*13*). For the Cys-360 mutants this spectral intermediate was due to the production of the off-pathway product PMP resulting from the protonation of the quinoid intermediate at C4′ instead of C_α following decarboxylation (Figure 1). Thus, these data suggest that F397A ODC is also catalyzing abortive transamination at an increased rate over the wild-type enzyme.

Single wavelength data were collected at 420 nm for a range of substrate concentrations (0.12−45 mM) to further analyze the pre-steady-state reaction. The data are minimally described by a two-step model and were fitted to eq 1 ($N = 2$) to obtain the observed rate constants. Both phases are dependent on the concentration of L-Orn. The first phase (increase at 420 nm) does not saturate in an experimentally accessible substrate range, while phase 2 (decrease at 420 nm) is fully saturated above 0.25 mM L-Orn. Attempts to fit the substrate dependence data to a simple linear two- or three-step model failed. The modeling suggests that additional steps or off-pathway events are required to describe the data, but given the small amplitude of phase 1, noise in the data, and only two observed transitions, inclusion of more steps in the model would require overfitting the data. HPLC analysis of the reaction products (below) demonstrates that the product is deaminated in 30% of the turnovers. Thus two competing reactions, formation of putrescine and formation of γ-aminobutyraldehyde, will both contribute to the observed spectral changes, and this finding may be the cause of the complexity observed in the data. Regardless, the spectral data are consistent with formation of a ketimine intermediate with a rate constant ($k_{obs2} = 0.079 \pm 0.003$), at saturating L-Orn concentration, which is the same as those observed in both the steady-state analysis and the single turnover analysis. This step is preceded by minimally one faster step ($k_{obs1} = 23 \pm 1$ s^{-1} at 22.5 mM Orn).

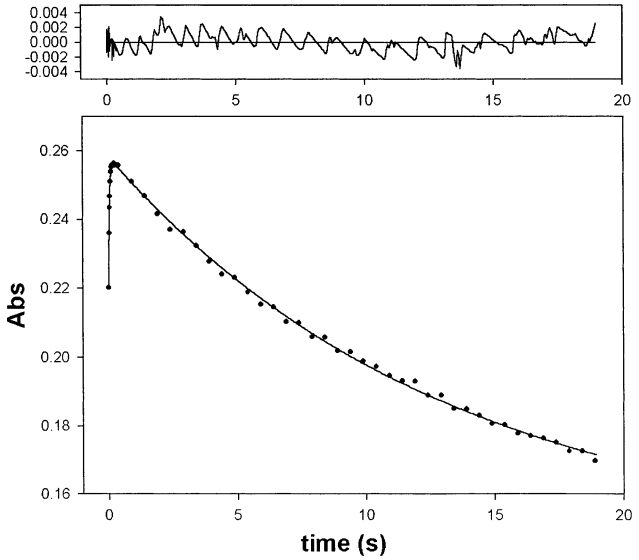

FIGURE 5: Single wavelength kinetic analysis of the reaction of F397A ODC with L-Orn. F397A ODC (40 μM) was mixed with L-Orn (22.5 mM), and the reaction was monitored at 420 nm. Data were fitted to eq 1 ($N = 2$) to obtain the observed rate constants for a two-step reaction process, where $k_{obs1} = 23 \pm 1$ s^{-1} and $k_{obs2} = 0.051 \pm 0.001$ s^{-1}. Data are displayed as filled circles, and the fit is displayed as a solid line. Residuals to the fit are displayed above the data plot.

These data support the conclusion that the single turnover kinetics, the steady-state kinetics, and the final observable step (k_{obs2}) from the pre-steady-state absorbance data are measuring the same reaction chemistry, which based on the single turnover data is likely to be the decarboxylation step (Table 1). The ketimine intermediate cannot form until after decarboxylation (Figure 1) and would not contribute to the single turnover rate. Thus, these data suggest either that decarboxylation and protonation occur in a concerted step or that the protonation step is fast relative to the decarboxylation step. These data provide no information about the rates of product release, because these steps follow the rate-determining step.

The fast step observed in the stopped-flow data likely represents substrate binding steps, which could include the formation of the Michaelis complex, the *gem*-diamine, and Schiff base species. For the wild-type enzyme, Schiff base formation is complete during the dead time of the mixer [rate > 1000 s^{-1} at 37 °C (*16*, *19*)]. Two steps were observed to precede decarboxylation for the Arg mutant of Lys-69, and a minimum of one step was observed for the Cys-360 mutant enzymes (*13*, *19*). The first observed step in the reaction of L-Orn with F397A ODC ($k_1 = 23$ s^{-1}) is minimally 40-fold slower than observed for the wild-type enzyme.

Chromatographic Determination of the Steady-State Rate of Product Formation by F397A ODC. Product formation catalyzed by the reaction of F397A ODC with L-Orn was analyzed by HPLC in the presence of excess PLP (Figure 6). If transamination occurs, the product of the reaction is PMP and γ-aminobutyraldehyde (γABA). Reduction of γABA with $NaBH_4$ yields the commercially available compound pyrrolidine, which allows the reaction to be standardized. The products of the reaction of L-Orn with F397A ODC were reduced with $NaBH_4$, and they were analyzed by HPLC after derivitization using the AccQ·TAG kit (Waters, Milford, MA). The overall steady-state rates of

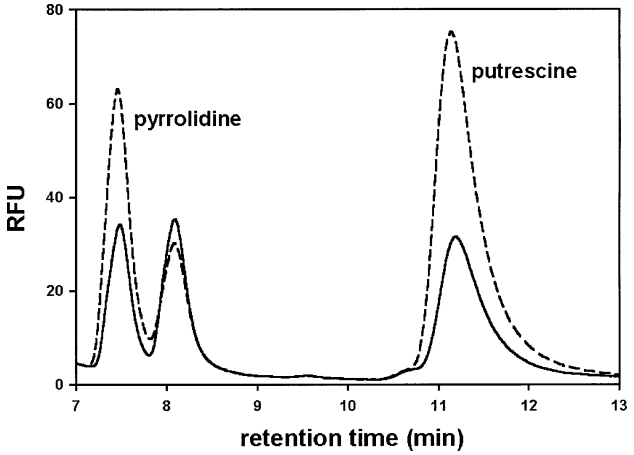

FIGURE 6: Representative HPLC analysis of product formation in the reaction of F397A ODC with L-Orn. Enzyme (60 μM) was incubated with substrate (3 mM) in the presence of excess PLP (3 mM) at 37 °C for various time points. The products of the reaction were derivatized and separated on an AccQ·Tag column (Experimental Procedures). The trace of the separated reaction products (RFU = relative fluorescence units versus retention time) is displayed for two representative reaction time points: 1 min (solid line) and 2 min (dashed line). Products are labeled above the corresponding peaks. The unlabeled peak is background and does not increase with increased incubation time. Kinetic constants were obtained by collecting peak areas for a range of reaction times, and the concentration of pyrrolidine (reduced γABA) or putrescine in the sample was determined by comparison to a standard curve of known concentrations.

putrescine and γABA formation were determined to be 0.029 s^{-1} and 0.015 s^{-1}, respectively, as described in Experimental Procedures (0.044 s^{-1} total product formation) (Table 1). Under these conditions 66% of the product formed was putrescine, while 34% of enzymatic turnovers resulted in formation of the off-pathway product γABA (measured as pyrrolidine). Wild-type ODC catalyzes abortive deamination in <0.01% of turnovers (*13*); thus, mutation of F397 to Ala resulted in a significant increase in off-pathway protonation events.

DISCUSSION

Enzymes can accelerate chemical reactions either by stabilizing the transition state or by destabilizing the ground state (*24*, *25*). PLP-dependent enzymes such as ODC utilize the electron-withdrawing properties of the PLP cofactor to stabilize reaction intermediates, thus lowering activation barriers (*4*). In these enzymes the apoenzyme facilitates proper orientation of the reacting groups relative to the π electrons of the cofactor to promote reactivity and control reaction specificity. In addition, the environment of the enzyme site that interacts with the leaving group could provide either stabilizing or destabilizing interactions to direct catalysis.

The X-ray structures of *T. brucei* ODC bound to decarboxylated DFMO (*12*) or to D-Orn (*20*) both suggest that the carboxylate of L-Orn will be bound in a buried pocket on the *re* face of the cofactor, formed by aromatic, hydrophobic, and negatively charged residues (Figure 2). Binding of the CO_2 leaving group on the *re* face of the cofactor has the additional advantage of placing the L-Orn C_α proton on the opposite face from Lys-69. The active site Lys residue is the catalytic base in enzymes that catalyze proton abstraction [e.g., aspartate aminotransferase (*26*−*28*) and alanine racemase (*29*)]. Thus placement of this proton away from a potential catalytic base disfavors proton abstraction, which would yield the incorrect reaction chemistry. Structural studies of the apoenzyme of L-Thr-*O*-3-phosphate decarboxylase bound to substrate also demonstrate that this enzyme places the carboxylate leaving group on the opposite face of the PLP cofactor from the catalytic Lys residue (*30*).

This model for L-Orn binding suggests that Phe-397 will form one of the dominant contacts between the enzyme and the CO_2 leaving group. In support of this hypothesis the data presented here demonstrate that mutation of Phe-397 to Ala reduces the rate of the decarboxylation step by 2100-fold. Further, while product release is rate limiting for wild-type ODC (*16*), the decarboxylation step has become rate limiting in the mutant enzyme. Thus Phe-397 plays an essential role in facilitating the decarboxylation step in ODC catalysis.

Phe-397 also contributes to the reaction fidelity of ODC. Mutation of Phe-397 to Ala resulted in a significant increase in off-pathway protonation events. The increased level of off-pathway transamination events observed in this mutant may result from greater access to the C4′ position by water or by poor positioning of a general acid required for correct protonation. Mutants of Cys-360, a residue required for correct protonation, have previously been demonstrated to undergo transamination in 90% of the catalytic events (*13*). The Cys-360 side chain may function as a general acid in the protonation step, and if so, loss of packing interactions between residues from the Phe-397 loop and the Cys-360 loop may disrupt the functioning of this residue.

The predicted carboxylate binding site on ODC is composed of hydrophobic and negatively charged or electron-rich residues, all of which would provide unfavorable interactions with the substrate carboxylate. This binding site would be expected to disfavor the negatively charged substrate carboxylate and to favor the more neutral transition state. Studies on model compounds have demonstrated a role for a nonpolar environment in promoting decarboxylation; the reaction rate was enhanced by several orders of magnitude in nonpolar solvent conditions (*31*, *32*). This mechanism for rate acceleration by enzymes is also supported by the demonstration of an increased decarboxylation rate upon binding of model substrates to the apolar environment of catalytic antibodies (*33*−*35*). In further support for ground-state destabilization on ODC, substrate has been demonstrated to bind 24-fold more weakly than product to a K69R mutant of ODC (*19*).

Similar to ODC, structural analysis of several other decarboxylases demonstrates that the carboxylate group either forms weak interactions with the enzyme or is bound in a hydrophobic or negatively charged pocket that would provide disfavorable interactions. The substrate carboxylate binding pocket in pyruvoyl-dependent histidine decarboxylase is predominantly hydrophobic and additionally contains a Glu residue (*38*). Orotidine 5′-monophosphate decarboxylase, unique in its ability to promote decarboxylation in the absence of a prosthetic cofactor, is thought to achieve catalytic rate acceleration by bringing the carboxylate leaving group into close proximity with an active site Asp residue (*39*, *40*). The large unfavorable repulsive effect upon binding is compensated for in this case by strong noncovalent

interactions with phosphate and ribose moieties of the substrate (*41*).

The destabilizing interactions observed in the α-carboxylate binding site of the decarboxylases differ from PLP enzymes that catalyze proton abstraction. These enzymes instead utilize the carboxylate as a binding determinant through the formation of stabilizing interactions in the active site. Aspartate aminotransferase forms ionic and hydrogen bond interactions with the α-carboxylate through interactions with active site Arg and Gly residues (*36*), and alanine racemase forms hydrogen bond interactions through active site residues and water (*37*). One novel example of a decarboxylase is dialkylglycine decarboxylase, a PLP-dependent enzyme that has the unusual burden of catalyzing both decarboxylation and transamination. This enzyme is reported to form multiple hydrogen-bonding interactions with the substrate carboxylate, though these contacts change depending on if the substrate is oriented for decarboxylation or proton abstraction (*6, 42*).

In summary, the data derived from the kinetic analysis of F397A ODC, combined with inferences drawn from *T. brucei* ODC crystal structures, support the hypothesis that the carboxyl leaving group of L-Orn is buried on the *re* face of the cofactor. The hydrophobic and electron-rich nature of this binding site promotes decarboxylation by destabilizing the charged carboxylate and favoring the electrostatically more neutral transition state.

REFERENCES

1. Bitoni, A. J., Bacchi, C. J., McCann, P. P., and Sjoerdsma, A. (1985) Catalytic irreversible inhibition of *Trypanosoma brucei brucei* ornithine decarboxylase by substrate and product analogs and their effects on murine trypanosomiasis, *Biochem. Pharmacol. 34*, 1773−1777.
2. Taelman, H., Schechter, P. J., Marcelis, L., Sonnet, J., Kazyumba, G., Dasnoy, J., Haegele, K. D., Sjoerdsma, A., and Wery, M. (1987) Difluoromethylornithine, an effective new treatment of Gambian trypanosomiasis, *Am. J. Med. 82*, 607−614.
3. Kuzoe, F. A. (1993) Current situation of African trypanosomiasis, *Acta Trop. 54* (3−4), 153−162.
4. Walsh, C. (1979) in *Enzymatic reactions requiring pyridoxal phosphate* (Bartlett, A. C., and McCombs, L. W., Eds.) pp 777−827, W. H. Freeman and Co., San Francisco.
5. Dunathan, H. C. (1966) Conformation and reaction specificity in pyridoxal phosphate enzymes, *Proc. Natl. Acad. Sci. U.S.A. 55*, 712−716.
6. Sun, S., Zabinski, R. F., and Toney, M. D. (1998) Reactions of alternate substrates demonstrate stereoelectronic control of reactivity in dialkylglycine decarboxylase, *Biochemistry 37*, 3865−3875.
7. McPhalen, C. A., Vincent, M. G., Picot, D., Jansonius, J. N., Lesk, A. M., and Chothia, C. (1992) Domain closure in mitochondrial aspartate aminotransferase, *J. Mol. Biol. 227*, 197−213.
8. Milne, J. J., and Malthouse, P. G. (1996) The effect of different amino acid side chains on the stereospecificity and catalytic efficiency of the tryptophan synthase-catalyzed exchange of the alpha-protons of amino acids, *Biochem. J. 314*, 787−791.
9. O'Leary, M. H., and Piazza, G. J. (1978) Specificity in enzymatic decarboxylation, *J. Am. Chem. Soc. 100*, 632−633.
10. Toney, M. D. (2001) Computational studies on nonenzymatic and enzymatic pyridoxal phosphate catalyzed decarboxylations of 2-aminoisobutyrate, *Biochemistry 40*, 1378−1384.
11. O'Leary, M. H., and Piazza, G. J. (1981) Medium effects in enzyme-catalyzed decarboxylations, *Biochemistry 20*, 2743−2748.
12. Grishin, N. V., Osterman, A. L., Brooks, H. B., and Phillips, M. A. (1999) X-ray structure of ornithine decarboxylase from *Trypanosoma brucei*: the native structure and the structure in complex with α-difluoromethylornithine, *Biochemistry 38*, 15174−15184.
13. Jackson, L. K., Brooks, H. B., Osterman, A. L., Goldsmith, E. J., and Phillips, M. A. (2000) Altering the reaction specificity of eukaryotic ornithine decarboxylase, *Biochemistry 39*, 11247−11257.
14. Kern, A. D., Olivera, M. A., Coffino, P., and Hackert, M. L. (1999) Structure of mammalian ornithine decarboxylase at 1.6 Å resolution: stereochemical implications of PLP-dependent amino acid decarboxylases, *Structure 7*, 567−581.
15. Almrud, J. J., Olivera, M. A., Kern, A. D., Grishin, N. V., Phillips, M. A., and Hackert, M. L. (2000) Crystal structure of human ornithine decarboxylase at 2.1 Å resolution: structural insights to antizyme binding, *J. Mol. Biol. 295*, 7−16.
16. Brooks, H. B., and Phillips, M. A. (1997) Characterization of the reaction mechanism for *Trypanosoma brucei* ornithine decarboxylase by multiwavelength stopped-flow spectroscopy, *Biochemistry 36*, 15147−15155.
17. Osterman, A. L., Kinch, L. N., Grishin, N. V., and Phillips, M. A. (1995) Acidic residues important for substrate binding and cofactor reactivity in eukaryotic ornithine decarboxylase identified by alanine scanning mutagenesis, *J. Biol. Chem. 270*, 11797−11802.
18. Osterman, A. L., Brooks, H. B., Rizo, J., and Phillips, M. A. (1997) Role of Arg-277 in the binding of pyridoxal 5′-phosphate to *Trypanosoma brucei* ornithine decarboxylase, *Biochemistry 36*, 4558−4567.
19. Osterman, A. L., Brooks, H. B., Jackson, L. K., Abbott, J. J., and Phillips, M. A. (1999) Lysine-69 plays a key role in catalysis by ornithine decarboxylase through acceleration of the Schiff base formation, decarboxylation, and product release steps, *Biochemistry 38*, 11814−11826.
20. Jackson, L. K., Goldsmith, E. J., and Phillips, M. A. (2003) X-ray structure determination of *Trypanosoma brucei* ornithine decarboxylase bound to D-ornithine and to G418: Insights into substrate binding and conformational flexibility (manuscript submitted for publication).
21. Pegg, A. E., McGovern, K. A., and Wiest, L. (1987) Decarboxylation of α-difluoromethylornithine by ornithine decarboxylase, *Biochem. J. 241*, 305−307.
22. Myers, D. P., Jackson, L. K., Ipe, V. G., Murphy, G. E., and Phillips, M. A. (2001) Long-range interactions in the dimer interface of ornithine decarboxylase are important for enzyme function, *Biochemistry 40*, 13230−13236.
23. Osterman, A., Grishin, N. V., Kinch, L. N., and Phillips, M. A. (1994) Formation of functional cross-species heterodimers of ornthine decarboxylase, *Biochemistry 33*, 13662−13667.
24. Fersht, A. (1977) *Enzyme Structure and Mechanism* (Fersht, A., Ed.) 2nd ed., W. H. Freeman and Co., New York.
25. Jencks, W. P. (1975) Binding energy, specificity, and enzymatic catalysis: the Circe effect, *Adv. Enzymol. 43*, 219−410.
26. Toney, M. D., and Kirsch, J. F. (1989) Direct Brønsted analysis of the restoration of activity to a mutant enzyme by exogenous amines, *Science 243*, 1485−1488.
27. Toney, M. D., and Kirsch, J. F. (1991) The K258R mutant of aspartate aminotransferase stabilizes the quinoid intermediate, *J. Biol. Chem. 266*, 23900−23903.
28. Toney, M. D., and Kirsch, J. F. (1993) Lysine 258 in aspartate aminotransferase: enforcer of the Circe effect for amino acid substrates and general-base catalyst for the 1,3-prototropic shift, *Biochemistry 32*, 1471−1479.
29. Watababe, A., Kurokawa, Y., Yoshimura, T., Kurihara, T., Soda, K., and Esaki, N. (1999) Role of lysine 39 of alanine racemase from *Bacillus stearothermophilus* that binds pyridoxal 5′-phosphate, *J. Biol. Chem. 274*, 4189−4194.
30. Cheong, C., Escalante-Semerena, J. C., and Rayment, I. (2002) Structural studies of the L-threonine-O-3-phosphate decarboxylase (CobD) enzyme from *Salmonella enterica*: The apo, substrate, and product-aldimine complexes, *Biochemistry 41*, 9079−9089.
31. Kemp, D. S., and Paul, K. G. (1975) The physical organic chemistry of benzisoxazoles. III. The mechanism and the effects of solvents on rates of decarboxylation of benzisoxazole-3-carboxylic acids, *J. Am. Chem. Soc. 97*, 7305−7312.
32. Kemp, D. S., Cox, D. D., and Paul, K. G. (1975) The physical organic chemistry of benzisoxazoles. IV. The origins and catalytic nature of the solvent rate acceleration for the decarboxylation of 3-carboxybenzisoxazoles, *J. Am. Chem. Soc. 97*, 7312−7318.
33. Lewis, C, Krämer, T., Robinson, S., and Hilvert, D. (1991) Medium effects in antibody-catalyzed reactions, *Science 253*, 1019−1022.

34. Ashley, J. A., Lo, C. L., McElhaney, G. P., Wirsching, P., and Janda, K. D. (1993) A catalytic antibody model for PLP-dependent decarboxylases, *J. Am. Chem. Soc. 115*, 2515−2516.
35. Lewis, C., Paneth, P., O'leary, M. H., and Hilvert, D. (1993) Carbon kinetic isotope effects on the spontaneous and antibody-catalyzed decarboxylation of 5-nitro-3-carboxybenzisoxazole, *J. Am. Chem. Soc. 115*, 1410−1413.
36. Rhee, S., Silva, M. M., Hyde, C. C., Rogers, P. H., Metzler, C. M., Metzler, D. E., and Arnone, A. (1997) Refinement and comparisons of the crystal structures of pig cytosolic aspartate aminotransferase and its complex with 2-methylaspartate, *J. Biol. Chem. 272*, 17293−17302.
37. Morollo, A. A., Petsco, G. A., and Ringe, D. (1999) Structure of a Michaelis complex analogue: propionate binds in the substrate carboxylate site of alanine racemase, *Biochemistry 38*, 3293−3301.
38. Gallagher, T., Snell, E. E., and Hackert, M. L. (1989) Pyruvoyl-dependent histidine decarboxylase, *J. Biol. Chem. 264*, 12737−12743.
39. Appleby, T. C., Kinsland, C., Begley, T. P., and Ealick, S. E. (2000) The crystal structure and mechanism of orotidine 5′-monophosphate decarboxylase, *Proc. Natl. Acad. Sci. U.S.A. 97*, 2005−2010.
40. Wu, N., Mo, Y., Gao, J., and Pai, E. F. (2000) Electrostatic stress in catalysis: structure and mechanism of the enzyme orotidine monophosphate decarboxylase, *Proc. Natl. Acad. Sci. U.S.A. 97*, 2017−2022.
41. Miller, B. G., Hassell, A. M., Wolfenden, R., Milburn, M. V., and Short, S. A. (2000) Anatomy of a proficient enzyme: The structure of orotidine 5′-monophosphate decarboxylase in the presence and absence of a potential transition state analog, *Proc. Natl. Acad. Sci. U.S.A. 97*, 2011−2016.
42. Toney, M. D., Hohenester, E., Keller, J. W., and Jansonius, J. N. (1995) Structural and mechanistic analysis of two refined crystal structures of the pyridoxal phosphate-dependent enzyme dialkylglycine decarboxylase, *J. Mol. Biol. 245*, 151−179.

BI026795Z